Reduction of Open-Circuit DC Winding Induced Voltage and Torque Pulsation in the Wound Field Switched Flux Machine by Stator Axial Pairing of Tooth-Tips

Wentao Zhang, Zhongze Wu*, Wei Hua, and Z. Q. Zhu

***Abstract* -- In this paper, stator axial pairing of tooth-tips is proposed to suppress the open-circuit DC winding induced voltage and torque pulsation in the wound field switched flux machine. The stator is divided into two segments axially, whilst these two segments have different tooth-tip arcs. The proposed technique can suppress the rated on-load torque ripple from 17.91% to 6.99%, reduce the peak-to-peak value of cogging torque from 5.14 Nm to 0.48 Nm, and reduce the open-circuit DC winding induced voltage at 1500 r/min from 39.79 V to 6.21 V. Although the efficiency of the machine is slightly reduced from 81.5% to 80.7%, the average electromagnetic torque can be maintained by >95%.**

***Index Terms*-- Axial pairing, cogging torque, DC winding induced voltage, wound field switched flux machine, tooth-tip, torque pulsation, torque ripple, wound field switched flux machine.**

I. Introduction

In recent years, non-permanent magnet (PM) machines have received considerable attention, which includes the switched reluctance machine (SRM), the synchronous reluctance machine (SynRM), and the wound field (WF) synchronous machine. The conventional wound-rotor synchronous machine has been widely applied in the electric power generation and the electric grid system. However, the further application of the wound-rotor synchronous machine is limited by the existence of slip ring and brush [1]. The wound field switched flux (WFSF) machine has both armature winding and DC winding in the stator, which achieves the brushless operation. Both the WFSF machine and the SRM have a robust and simple rotor. Compared with the SRM, the WFSF machine shows a higher torque density and a lower torque ripple [2]. Fig. 1 shows the cross-section of the 12-slot/10-pole WFSF machine.

The WFSF machine has received much attention recently. A single phase low cost WFSF machine is introduced in [3]. In [4], a partionated stator WFSF (PS-WFSF) machine with the DC winding and the armature winding placed in separate stators is analysed. It shows that the PS-WFSF machine has a higher torque density than the conventional WFSF machine. The analytical approaches for predicting the open-circuit and armature reaction performances of the WFSF machine are proposed in [5] and [6], respectively.

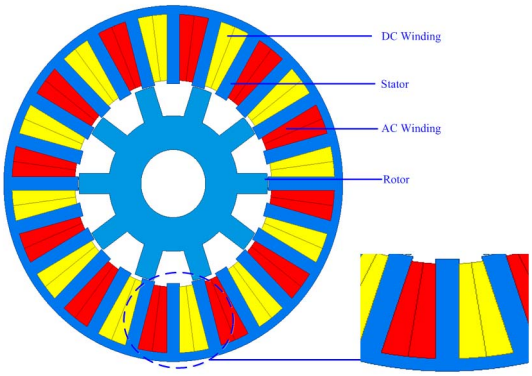

(a)

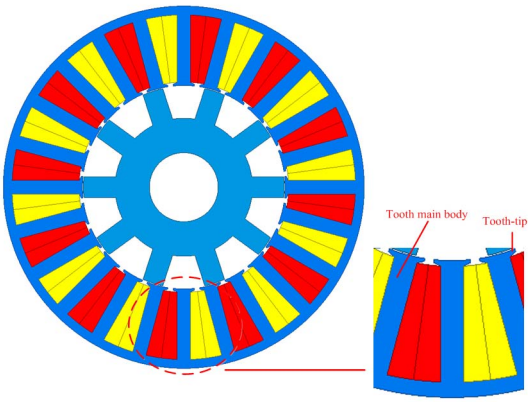

(b)

Fig. 1. Cross-section of the WFSF machine. (a) Without tooth-tip (b) With tooth-tips.

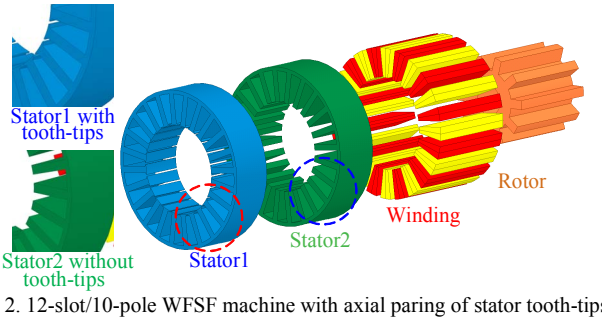

Fig. 2. 12-slot/10-pole WFSF machine with axial paring of stator tooth-tips.

This work was supported in part by the National Natural Science Foundation of China under Grant 51825701 and the key R&D program of Jiangsu Province (BE2019073).

Wentao Zhang and Wei Hua are with School of Electrical Engineering, Southeast University, Nanjing 210096, China (email: zhangwentaoseu@outlook.com; huawei1978@seu.edu.cn).

Zhongze Wu is with The Institute for Advanced Automotive Propulsion Systems (IAAPS), Department of Mechanical Engineering, University of Bath, Bath BA2 7AY, U.K. (email: z.wu@bath.ac.uk).

Z. Q. Zhu is with Department of Electronic and Electrical Engineering, University of Sheffield, Sheffield S10 2TN, U.K. (email: z.q.zhu@sheffield.ac.uk).

It is found in [7] and [8] that due to the variation of the air-gap permeance, the induced voltage pulsation will be produced in the DC winding, which is a challenge for the power supply and could deterioate the control performance. Reduction methods including skewing [7], [8], chamfering [9], rotor tooth arc pairing [10] and rotor axial pairing [9] have been proposed to reduce the DC winding induced voltage pulsation and verified by finite element (FE) and / or experimental results.

This paper proposes a torque pulsation and open-circuit DC winding induced voltage reduction method for the WFSF machine using the stator axial pairing of the tooth-tips (see Fig. 2). The stator is divided into two segments axially, whilst these two segments have different tooth-tip arcs with zero tooth-tip arc case included, i.e. without tooth-tip. It is worth noting that the only difference between these two segments of the stator is the tooth-tip arc. Therefore, it is necessary to figure out the influence of the tooth-tip on WFSF machine firstly. The influence of the tooth-tip in various machines has been well investigated, including surface-mounted PM machines [11], [12], interior PM machines [13] and induction machines [14].

This paper is organized as follows. In section II, the topology of the WFSF machine and the design illustration are given. Section III firstly gives the sensitivity analysis of the stator tooth-tips, and then the influence of stator tooth-tips on the torque pulsation and the open-circuit DC winding induced voltage of the WFSF machine is introduced. In section IV, the principle of the axial pairing and the procedure to choose the key parameters are given. Electromagnetic performance comparison results among four WFSF machines are also given, including two machines using the stator axial pairing of tooth-tips and the other two with / without tooth-tips.

II. Machine Topology

Different from the original WFSF machine without tooth-tip shown in Fig. 1(a), the stator of the WFSF machine using the proposed axial pairing method is divided into two segments axially, whilst these two segments have different tooth-tip arcs. The illustration of the dimensional parameters of the stator with tooth-tips is given in Fig. 3. Detailed design parameters are given in Table I.

The design parameters in Table I are globally optimized to obtain the highest average electromagnetic torque. During the optimization, the current advanced angle is fixed as 0, i.e. zero d-axis current control i_d=0, since the reluctance torque is very small due to the similar d- and q-axis inductances in the WFSF machines [15]. It is worth noting that during the optimization process, the current density in both armature winding and DC winding are fixed as 5 Arms/mm^2. The slot filling factor for both armature and DC windings are fixed as 0.462, whilst the influence of tooth-tips on the slot area is not accounted here. When the magnetic saturation in the core is neglected, the armature winding slot area should be equal to the DC winding slot area to obtain the maximum average electromagnetic torque.

It should be noted that the tooth-tip is not introduced in the optimization, since the WFSF machine with stator tooth-tips exhibits a lower average torque than that without the stator tooth-tip, as shown in Fig. 4.

Table I
Design Parameters of the 12-Slot/10-Pole WFSF Machine Without the Tooth-Tip

Item	Unit	WFSF
Stack length, l_s	mm	120
Outer radius of stator, R_{so}	mm	105
Inner radius of rotor, R_{ri}	mm	20
Yoke radius of rotor, R_{ry}	mm	40
Single side width of air-gap, g	mm	0.5
Yoke radius of stator, R_{sy}	mm	99.85
Inner radius of stator, R_{si}	mm	58.94
Arc of stator tooth, θ_{st}	°	7.78
Arc of stator slot for coils, θ_{ss}	°	7.22
Arc of rotor pole, θ_{rp}	°	11.9
Number of turns per coil, N_w	-	24
Winding current density, J_s	Arms/mm^2	5
Rated rotor speed, Ω_r	r/min	1500
Rated torque, T_r	Nm	40.11
Rated power, P_r	kW	6.3
Efficiency, η	%	81.51

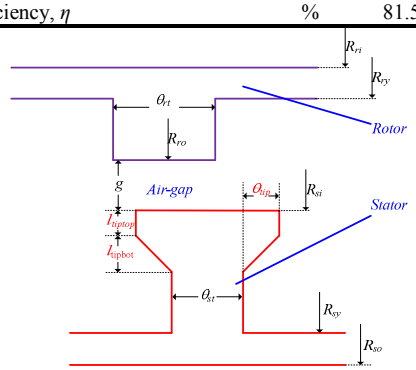

Fig. 3. Linear illustration of the dimensional parameters.

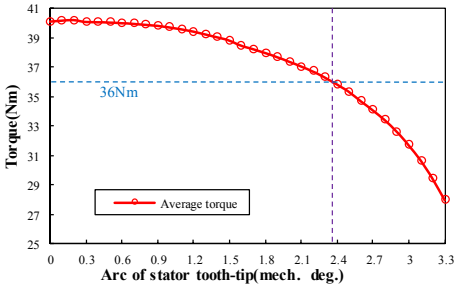

Fig. 4. Variation of 2-D FE predicted average electromagnetic torque with the stator tooth-tip angle θ_{tip} (BLAC, i_d=0, i_q=24.59A).

III. Influence of the Stator Tooth-Tips

The topology of the stator tooth-tips in the WFSF machine is shown in Fig. 3, and the design parameters are marked red, i.e. arc of the tooth-tip θ_{tip}, tooth-tip top length l_{tiptop} and tooth-tip bottom length l_{tipbot}. Before analyzing the influence of the design parameters of the tooth-tips, the sensitivity analysis will wipe out the parameters that are not sensitive to the torque pulsation and the open-circuit DC winding induced voltage.

A. Sensitivity Analysis

The variation range of the tooth-tip design parameters are shown in Table II. It is worth noting that if the value of l_{tiptop} and l_{tipbot} are chosen around 0, *i.e.* a thin stator tooth-tip which is fragile and suffers from manufacturing difficulty, tooth-tips will suffer from a strong magnetic saturation. Drastic performance variation of the WFSF machine will occur, which

is not meaningful practically but will affect the sensitivity analysis. Therefore, the starting point of the variation range for l_{tiptop} and l_{tipbot} is set as 1mm to avoid this, as shown in TABLE II.

TABLE II
VARIATION RANGE OF DESIGN VARIABLES OF THE STATOR TOOTH-TIPS

Design variables	Variation range
Arc of tooth-tip, θ_{tip}	[0 deg, 3.5 deg]
Tooth-tip top length, l_{tiptop}	[1 mm, 3 mm]
Tooth-tip bottom length, l_{tipbot}	[1 mm, 3 mm]

TABLE III
TOTAL EFFECT INDEX OF DESIGN VARIABLES OF THE STATOR TOOTH-TIPS

Design variables	Analysis objectives		
	T_{rip}	T_{cog}	E_{ff}
Arc of Tooth-tip, θ_{tip}	0.296	0.058	0.816
Tooth-tip top length, l_{tiptop}	0.003	0.009	0.018
Tooth-tip bottom length, l_{tipbot}	0.008	0.050	0.143

The sensitivity analysis uses the torque ripple T_{rip}, peak-to-peak value of cogging torque T_{cog} and open-circuit DC winding induced voltage E_{ff} at the rated rotor speed 1500 r/min as the sensitivity analysis objectives. The torque ripple T_{rip} in this paper is defined as the ratio of the peak-to-peak value of the electromagnetic torque to its average value T_{avg}.

The sensitivity level is given by the total-effect index S_{Ti}, which is expressed as,

$$S_{Ti} = \frac{E_{X\sim i}\left(Var_{X_i}(Y|X_{\sim i})\right)}{Var(Y)} \tag{2}$$

where $X_{\sim i}$ and Y are the input and output of the model, respectively. $Var(Y)$ is the variance of the output and $Var_{Xi}(Y|X_{\sim i})$ is the variance of the output caused by input $X_{\sim i}$. $E_{X\sim i}(Var_{Xi}(Y|X_{\sim i}))$ means the sum of $Var_{Xi}(Y|X_{\sim i})$. Monte Carlo estimators are used to calculate S_{Ti} [16], [17], which can be expressed as,

$$S_{Ti} = \frac{E_{X\sim i}\left(Var_{X_i}(Y|X_{\sim i})\right)}{Var(Y)} \approx \frac{1}{2N}\frac{\sum_{j=1}^{N}\left(f(A)_j - f\left(A_B^i\right)_j\right)^2}{Var(Y)} \tag{3}$$

where A and B are input parameter sequence used to test the output of the model.

The total effect indexes for various analysis objectives are given in TABLE III. For all the three analysis objectives, θ_{tip} obtains the highest total effect index, which means that θ_{tip} is most sensitive to T_{rip}, T_{cog} and E_{ff}. It should be noted that for the cogging torque, the total effect index of l_{tipbot} is 0.050, which is slightly smaller than the index of θ_{tip}. That is caused by some special conditions, i.e. non-ignorable flux leakage, unperfect mesh of the FE model, *etc*.

B. Torque Pulsation

The tooth-tip has been widely used in torque pulsation reduction [18]. However, the influence of tooth-tips on the torque pulsation of the WFSF machine has not been fully investigated. In Fig. 5, the variation of the torque ripple and cogging torque with θ_{tip} is predicted by 2-D FE. Introduction of tooth-tip can reduce the cogging torque from 5.14 Nm to 2.20 Nm, and reduce the torque ripple from 17.91% to 13.71%. However, the average torque can only be maintained by 86.5% of the original value when the torque ripple is maximally suppressed.

Torque pulsation is contributed by the harmonic torque components, including the on-load torque ripple and the cogging torque. Both the on-load torque and the cogging torque can be expressed in Fourier series as,

$$T_e(\theta_m) = T_{avg} + \sum_{i=1}^{\infty} T_{ei}\cos(iN_r\theta + \theta_{ei}) \tag{4}$$

$$T_{cog}(\theta_m) = \sum_{j=1}^{\infty} T_{cogj}\,cos\left(jN_r\theta + \theta_{cogj}\right) \tag{5}$$

where θ_m is rotor mechanical position, N_r is the rotor pole number, T_{ei} is magnitude of the i^{th} on-load torque harmonic and θ_{ei} is the initial phase of the i^{th} on-load torque harmonic. T_{cogj} is magnitude of the j^{th} cogging torque harmonic and θ_{cogj} is the initial phase of the j^{th} cogging torque harmonic.

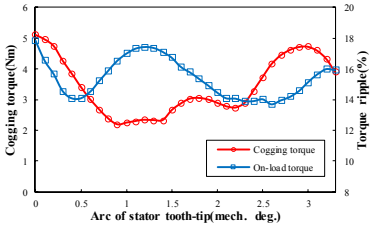

Fig. 5. 2-D FE predicted variation of T_{rip} and T_{cog} with θ_{tip}.

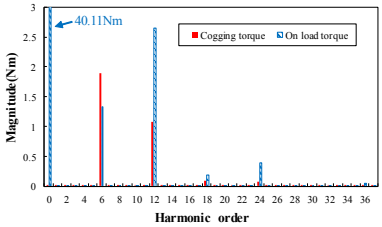

Fig. 6. 2-D FE predicted harmonic orders of the cogging torque and on-load torque of the WFSF machine without tooth-tip.

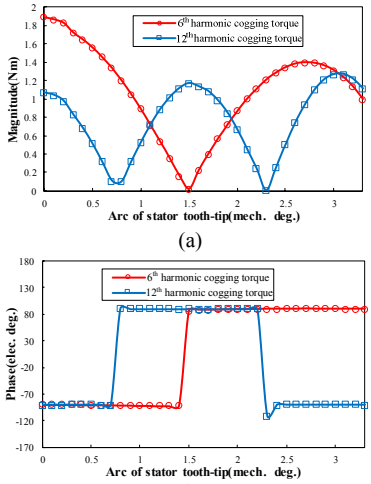

Fig. 7. 2-D FE predicted FFT results of 6th and 12th cogging torque harmonics with various θ_{tip}. (a) Magnitude of cogging torque (b) Phase of cogging torque.

Fig. 6 shows the FFT analysis results of both cogging torque and on-load torque of the analyzed machine without tooth-tips. Fig. 7 shows the FFT results of main harmonic components of cogging torque, including magnitude and phase. It is found that the phase of 6th and 12th harmonic components will change from -90 electric degrees to 90 electric degrees when the magnitude of the corresponding harmonic component approaches 0. Although the analytical model can explain this tendency [19], it cannot predict the value of θ_{tip} eliminating the certain order cogging torque harmonic. That is caused by the sever local magnetic saturation and flux leakage. Therefore, this paper uses 2-D FE

to predict the variation of cogging torque with the stator tooth-tip arc θ_{tip}.

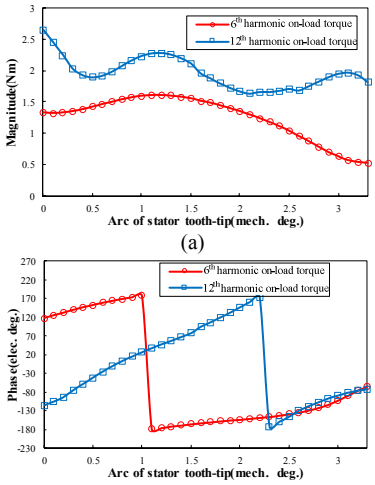

Fig. 8. 2-D FE predicted FFT results of 6th and 12th on-load torque harmonics with various θ_{tip}. (a) Magnitude of on-load torque (b) Phase of on-load torque.

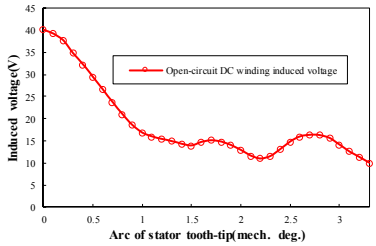

Fig. 9. 2-D FE predicted variation of E_{ff} pulsation with θ_{tip} when the WFSF machine operates at 1500 r/min.

Fig. 8 shows the FFT results of main harmonic components of the on-load torque, including magnitude and phase. The phase angle of harmonic components is proportional to the arc of stator tooth-tips. However, if the average torque is maintained by >90% of the original value, i.e. keeping θ_{tip}<2.3deg, the magnitude of 6th harmonic component will only change from 1.32 Nm to 1.17 Nm and that of the 12th harmonic component will change from 2.64 Nm to 1.66 Nm.

C. *Open-circuit DC Winding Induced Voltage*

The open-circuit DC winding induced voltage is produced by the variation of the open-circuit DC winding flux linkage, which can be expressed as [13],

$$E_{ff} = -\frac{d\psi_{ff}}{dt} \tag{6}$$

where E_{ff} is the open-circuit DC winding induced voltage and ψ_{ff} is the open-circuit DC winding flux linkage. The open-circuit DC winding induced voltage can also be expressed in Fourier series,

$$E_{ff} = \sum_{j=1}^{\infty} E_{ffj}\cos\left(jN_r\theta + \theta_{ffj}\right) \tag{7}$$

where E_{ffj} and θ_{ffj} are the magnitude and initial phase of i^{th} harmonic component of the open-circuit DC winding induced voltage, respectively.

Fig. 9 shows the variation of E_{ff} pulsation with θ_{tip}, where the E_{ff} pulsation can be reduced from 39.79 V to 11.0 V. It is shown that the tooth-tip is effective in reducing E_{ff}, however, the average torque will be sacrificed by 9% (see Fig. 4).

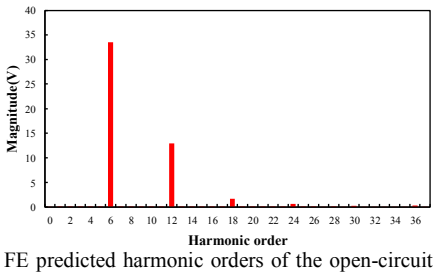

Fig. 10. 2-D FE predicted harmonic orders of the open-circuit DC winding induced voltage.

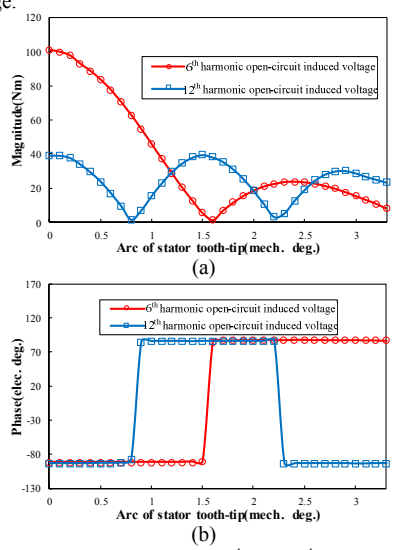

Fig. 11. 2-D FE predicted FFT results of 6th and 12th open-circuit DC winding induced voltage harmonics with various θ_{tip}. (a) Magnitude of induced voltage (b) Phase of induced voltage.

It is found in Fig. 10 that $6k^{th}$ (k=1,2,3,…) harmonic component are the main harmonic component of the open-circuit induced voltage. Fig. 11 shows the FFT results of main harmonic component of open-circuit DC winding induced voltage, including both magnitude and phase.

The phase of each main harmonic component will change from -92 electric degrees to 86 electric degrees, when the magnitude of corresponding harmonic component approaches 0, which is similar with the trend of the cogging torque shown in Fig. 7.

IV. Stator Axial Pairing of Tooth-Tips

Axial pairing is a method using the canceling effect to suppress the harmonic component, including the torque pulsation [9] and the DC winding induced voltage [20], [21]. It is shown in Fig. 12 that the two segments of the stator share a same center line of stator tooth. There is no shift angle between them, which is different from stator step skewing.

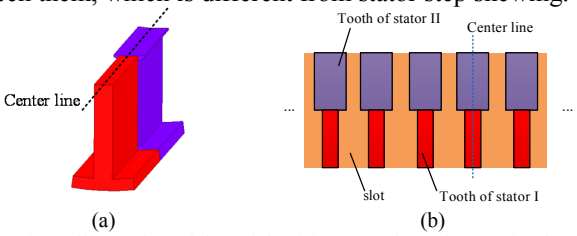

Fig. 12. Linear illustration of the axial pairing. (a) View of one pair of stator tooth (b) View of displacement of two segments of stator using axial pairing.

A. *Principle*

The open-circuit DC winding induced voltage and torque can be expressed in Fourier series (see equations (4), (5) and

(7)). The principle of axial pairing is based on the fact that the stator is divided into two parts axially and each part will produce DC winding induced voltage and torque separately. The torque of the WFSF machine using axial pairing T_{esum} can be expressed as,

$$T_{esum}(\theta) = T_1(\theta) + T_2(\theta) = T_{avg} + \sum_{i=1}^{\infty}[l_{s1}T_{1i}\cos(iN_r\theta + \theta_{1i}) + l_{s2}T_{2i}\cos(iN_r\theta + \theta_{2i})] \quad (8)$$

where T_{1i} and T_{2i} is the magnitude of i^{th} harmonic component of stator segment 1 and segment 2, respectively, whilst θ_{1i} and θ_{2i} are the corresponding phases. l_{s1} and l_{s2} are the length of two stator segments, respectively. According to the characteristics of quadratic function (Equation (8) can be rewritten as quadratic function related with l_{s1}), the i^{th} harmonic component can be suppressed maximally as,

$$\begin{cases} T_{imin} = \begin{cases} \dfrac{l_{stk}T_{1i}T_{2i}\sqrt{1-\cos^2(\theta_{1i}-\theta_{2i})}}{\sqrt{T_{1i}^2+T_{2i}^2-2T_{1i}T_{2i}\cos(\theta_{1i}-\theta_{2i})}}, 0 \le l_{s1}^* \le 1 \\ T_{1i} \quad , l_{s1}^* > 1 \\ T_{2i} \quad , l_{s1}^* < 0 \end{cases} \\ l_{s1}^* = \dfrac{T_{2i}^2 - T_{1i}T_{2i}\cos(\theta_{1i}-\theta_{2i})}{T_{1i}^2+T_{2i}^2-2T_{1i}T_{2i}\cos(\theta_{1i}-\theta_{2i})} l_{stk} \end{cases} \quad (9)$$

where T_{imin} is the minimal value of i^{th} harmonic component and l^*_{s1} is the analytically best length ratio for stator segment which yield $T_1(\theta)$. Physically $l^*_{s1} \in [0,1]$, which corresponds to the first condition in equation (9). Otherwise, l_{s1} should choose 0 or l_{stk}, which corresponds to the other two conditions. Such analysis is the same for i^{th} harmonic DC winding induced voltage. The equation (9) shows that magnitude and initial phase of the harmonic components produced by the two stator segments are the key parameters in suppressing the torque pulsation or the open-circuit DC winding induced voltage.

The initial phase can be controlled by θ_{tip}, as analyzed in section III. The magnitude can also be controlled by the length ratio between the two parts of the stator, which is defined as,

$$k_l = \frac{l_{s1}}{l_{s2}} \quad (10)$$

B. Procedure to Choose Parameters

Two types of axial pairing are introduced in this paper. One type is called axial pairing-I has one stator segment with a straight tooth and another stator segment with tooth-tips. Another type is named as axial pairing-II, in which both stator segments have tooth-tips but with different arcs.

In order to choose an appropriate θ_{tip} for the machine with tooth-tips. An optimization index H is defined as,

$$H(\theta_{tip}) = \lambda_1 T^*_{rip} + \lambda_2 T^*_{cog} + \lambda_3 E^*_{ff} - \lambda_4 T^*_{avg} \quad (11)$$

where λ_1, λ_2, λ_3 and λ_4 are weight of the objectives which is manually fixed at 2.5, 1, 1 and 2.5, respectively. This means the on-load performance is attached more importance in the optimization. T^*_{rip}, T^*_{cog}, E^*_{ff}, and T^*_{avg} are the normalized T_{rip}, T_{cog}, E_{ff} and T_{avg}, respectively.

As shown in Fig. 13, where θ_{tip} equals to 2.2 mechanical degrees (point P_1), the corresponding WFSF machine has the smallest value of H. However, the average torque will be 8.5% sacrificed (Fig. 4). In order to maintain the average torque by >95%, the other θ_{tip} (P_{optim} in Fig. 13), which also obtains the peak value of H and equals to 0.9 mechanical degrees, is chosen for the machine with tooth-tips.

The parameters chosen for the WFSF machines using axial pairing is a multi-variable and multi-objective optimization, and this paper uses the multi-objective genetic algorithm to choose the parameters combination.

The optimization functions and constraints for axial pairing-I are given as follows.

$$\begin{cases} function: \begin{bmatrix} min(E^*_{ff}), min(T^*_{rip}), \\ min(T^*_{cog}), max(T^*_{avg}) \end{bmatrix} \\ Constraints: \quad \theta_{tip} = 0.1deg, 0.2deg, \ldots. \end{cases} \quad (12)$$

Fig. 14 shows the feasible points of the WFSF machine using axial pairing-I. The color of the design points represents the value of normalized average torque. The optimal design is chosen on the pareto front surface. The choice of the solution depends on the importance of each objective [22], [23]. It should be noted that the optimized machine (k_l=0.4, θ_{tip}=1.5deg), which is marked in Fig. 14, can reduce T_{rip} from 17.91% to 7.44%, reduce T_{cog} from 5.14 Nm to 1.88 Nm and reduce E_{ff} from 39.79 V to 15.86 V.

The optimization functions and constraints for axial pairing-II is given as follows,

$$\begin{cases} function: \quad \begin{bmatrix} min(E^*_{ff}), min(T^*_{rip}), \\ min(T^*_{cog}), max(T^*_{avg}) \end{bmatrix} \\ Constraints: \begin{cases} \theta_{tip1}, \theta_{tip2} = 0.1deg, 0.2deg, \ldots \\ \theta_{tip1} < \theta_{tip2} \end{cases} \end{cases} \quad (13)$$

where θ_{tip1} and θ_{tip2} are the tooth-tip arcs for two stator segments, respectively.

Fig. 15 shows the feasible points of the WFSF machine using axial pairing-II. The optimized machine (k_l=0.4, θ_{tip1}=0.6deg, θ_{tip2}=2.1deg) is chosen at the pareto front surface. It can reduce T_{rip} from 17.91% to 6.99%, reduce T_{cog} from 5.14 Nm to 0.48 Nm and reduce E_{ff} from 39.79 V to 6.21 V.

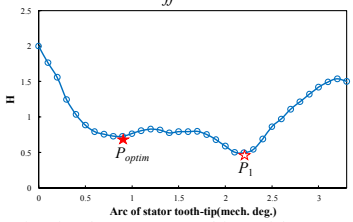

Fig. 13. Variation of H for the WFSF machine with stator tooth-tip arc.

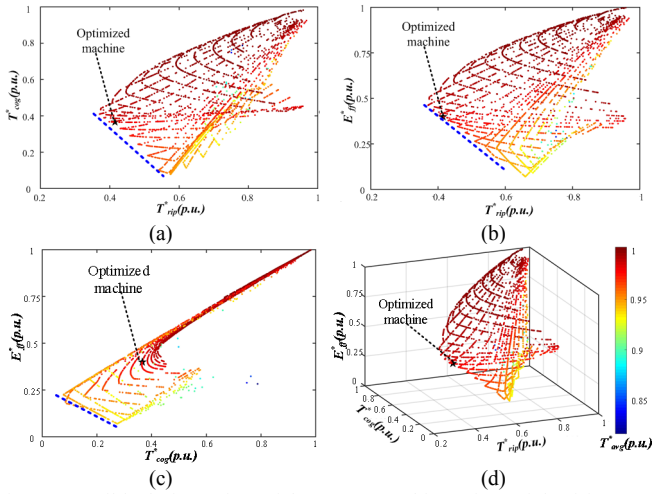

Fig. 14. Feasible design points of the WFSF machine using axial pairing-I. (a) T^*_{rip} to T^*_{cog} view (b) T^*_{rip} to E^*_{ff} view (c) T^*_{cog} to E^*_{ff} view (d) 3D view.

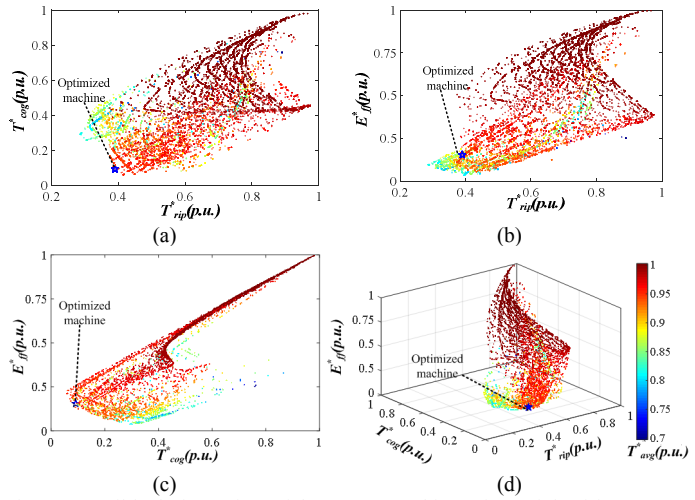

Fig. 15. Feasible design points of the WFSF machine using axial pairing-II. (a) T^*_{rip} to T^*_{cog} view (b) T^*_{rip} to E^*_{ff} view (c) T^*_{cog} to E^*_{ff} view (d) 3D view.

C. Comparison of Four WFSF Machines

The comparison constraint of the four WFSF machines is shown as follows,

1) Same design parameters shown in TABLE I.

2) Different stator tooth topologies which are listed as,

i) stator tooth without tooth-tips, i.e. straight tooth; ii) stator tooth with tooth-tips (θ_{tip}=0.9deg); iii) axial pairing-I of two segments of stators with one segment has a straight tooth, whilst another one is with tooth-tips (θ_{tip}=1.5 deg), and the length ratio k_l = 0.4; and iv) axial pairing-II of two segments of stators. Both segments have stator tooth-tips (θ_{tip1}=0.6 deg, θ_{tip2}=2.1 deg), whist the length ratio k_l =0.4.

As shown in Fig. 16, the WFSF machine using axial pairing-I and axial pairing-II show significant lower torque ripple of 7.44% and 6.95%, respectively, whilst the torque ripple of the WFSF machines without and with tooth-tips are 17.91% and 16.61%, respectively. Compared with the original machine without tooth-tip, T_{cog} and E_{ff} of the WFSF machine using stator axial pairing-II can be reduced by 90.66% and 84.39%, respectively.

The detailed comparison data of four machines are listed in TABLE IV. It is found that the WFSF machine using the proposed technique can effectively suppress torque ripple, cogging torque and open-circuit DC winding induced voltage, whilst the average torque can maintain by >95% and the efficiency is slightly reduced.

It is worth noting that axial pairing-II shows a greater reduction of torque pulsation and open-circuit DC winding induced voltage, as shown in TABLE IV. However, the average torque is more sacrificed.

TABLE IV
CHARACTERISTIC OF OPEN-CIRCUIT INDUCED VOLTAGE PULSATION, TORQUE RIPPLE, COGGING TORQUE AND EFFICIENCY

Item	Unit	Without tooth-tip	With tooth-tips	Axial pairing-I	Axial pairing-II
T_{avg}	Nm	40.11	39.85	39.36	38.24
T_{rip}	%	17.91	16.61	**7.44**	**6.99**
E_{ff}	V	39.79	18.51	15.86	6.21
T_{cog}	Nm	5.14	2.20	1.88	0.48
ΔT_{avg}	%	-	0.65%	1.89%	4.66%
ΔT_{cog}	%	-	57.2%	**63.4%**	**90.66%**
ΔE_{ff}	%	-	53.4%	**60.2%**	**84.39%**
η	%	81.5%	81.4%	81.2%	80.7%

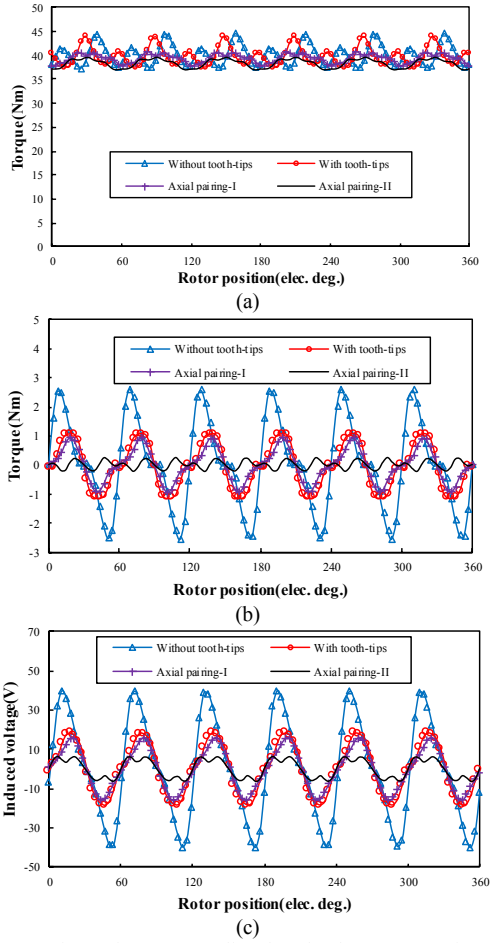

Fig. 16. Comparison of 2-D FE predicted on-load torque, cogging torque and open-circuit DC winding induced voltage of four machines. (a) On-load torque T_{avg} (b) Cogging torque T_{cog} (c) Open-circuit DC winding induced voltage E_{ff}.

V. CONCLUSION

In this paper, a torque pulsation and open-circuit DC winding induced voltage reduction method by stator axial pairing of tooth-tips is proposed for the WFSF machine. The stator of the WFSF machine using axial pairing is divided into two segments axially, whilst two segments have different tooth-tip arcs.

The influence of tooth-tips on the torque and open-circuit DC winding induced voltage is analyzed. The variation of main harmonic components, including magnitude and phase, are analyzed with various arc of stator tooth-tips.

The principle of stator axial pairing is introduced and key parameters, stator length ratio k_l and arc of stator tooth-tips θ_{tip} are chosen through the FE analysis results. FE results show that axial pairing can effectively suppress the torque pulsation and open-circuit DC winding induced voltage pulsation while maintain the average torque by >95% despite the efficiency of WFSF machine is slightly reduced.

VI. REFERENCES

[1] J. D. Widmer, R. Martin, and M. Kimiabeigi, 'Electric vehicle traction motors without rare earth magnets', *Sustainable Materials and Technologies*, vol. 3, pp. 7–13, Apr. 2015, doi: 10.1016/j.susmat.2015.02.001.

[2] G. Zhao, W. Hua, and J. Qi, 'Comparative Study of Wound-Field Flux-Switching Machines and Switched Reluctance Machines', *IEEE*

Transactions on Industry Applications, vol. 55, no. 3, pp. 2581–2591, May 2019, doi: 10.1109/TIA.2019.2892362.

[3] J. T. Chen, Z. Q. Zhu, S. Iwasaki, and R. Deodhar, 'Low cost flux-switching brushless AC machines', in *2010 IEEE Vehicle Power and Propulsion Conference*, Sep. 2010, pp. 1–6, doi: 10.1109/VPPC.2010.5728984.

[4] Z. Q. Zhu, Z. Z. Wu, D. J. Evans, and W. Q. Chu, 'A Wound Field Switched Flux Machine With Field and Armature Windings Separately Wound in Double Stators', *IEEE Transactions on Energy Conversion*, vol. 30, no. 2, pp. 772–783, Jun. 2015, doi: 10.1109/TEC.2014.2366993.

[5] B. Gaussens, E. Hoang, O. de la Barriere, J. Saint-Michel, M. Lecrivain, and M. Gabsi, 'Analytical Approach for Air-Gap Modeling of Field-Excited Flux-Switching Machine: No-Load Operation', *IEEE Transactions on Magnetics*, vol. 48, no. 9, pp. 2505–2517, Sep. 2012, doi: 10.1109/TMAG.2012.2196706.

[6] B. Gaussens *et al.*, 'Analytical Armature Reaction Field Prediction in Field-Excited Flux-Switching Machines Using an Exact Relative Permeance Function', *IEEE Transactions on Magnetics*, vol. 49, no. 1, pp. 628–641, Jan. 2013, doi: 10.1109/TMAG.2012.2211886.

[7] Z. Z. Wu, Z. Q. Zhu, C. Wang, J. C. Mipo, S. Personnaz, and P. Farah, 'Reduction of Open-Circuit DC-Winding-Induced Voltage in Wound Field Switched Flux Machines by Skewing', *IEEE Transactions on Industrial Electronics*, vol. 66, no. 3, pp. 1715–1726, Mar. 2019, doi: 10.1109/TIE.2018.2838106.

[8] Z. Wu, Z.-Q. Zhu, C. Wang, J.-C. Mipo, S. Personnaz, and P. Farah, 'Analysis and Reduction of On-Load DC Winding Induced Voltage in Wound Field Switched Flux Machines', *IEEE Trans. Ind. Electron.*, vol. 67, no. 4, pp. 2655–2666, Apr. 2020, doi: 10.1109/TIE.2019.2912779.

[9] Z. Wu *et al.*, 'Analysis and Suppression of Induced Voltage Pulsation in DC Winding of Five-Phase Wound-Field Switched Flux Machines', *IEEE Trans. Energy Convers.*, vol. 34, no. 4, pp. 1890–1905, Dec. 2019, doi: 10.1109/TEC.2019.2938161.

[10] Z. Wu, Z.-Q. Zhu, C. Wang, J.-C. Mipo, S. Personnaz, and P. Farah, 'Analysis and Reduction of On-Load DC Winding Induced Voltage in Wound Field Switched Flux Machines', *IEEE Trans. Ind. Electron.*, vol. 67, no. 4, pp. 2655–2666, Apr. 2020, doi: 10.1109/TIE.2019.2912779.

[11] D. Wu, Z. Q. Zhu, and W. Q. Chu, 'On-load performance of fractional slot SPM machines considering tooth-tip local magnetic saturation', in *2016 XXII International Conference on Electrical Machines (ICEM)*, Lausanne, Switzerland, Sep. 2016, pp. 506–512, doi: 10.1109/ICELMACH.2016.7732573.

[12] D. Wu, Z. Q. Zhu, and W. Q. Chu, 'Iron Loss in Surface-Mounted PM Machines Considering Tooth-Tip Local Magnetic Saturation', in *2016 IEEE Vehicle Power and Propulsion Conference (VPPC)*, Hangzhou, China, Oct. 2016, pp. 1–6, doi: 10.1109/VPPC.2016.7791717.

[13] D. Wu, Z. Q. Zhu, and W. Chu, 'Reduction of On-Load Terminal Voltage Distortion in Fractional Slot Interior Permanent Magnet Machines', *IEEE Transactions on Energy Conversion*, vol. 31, no. 3, pp. 1161–1169, Sep. 2016, doi: 10.1109/TEC.2016.2540620.

[14] L. CigAnek, 'Air Gap Field Under the Saturated Tooth of an Induction Motor', *IEEE Transactions on Power Apparatus and Systems*, vol. PAS-87, no. 11, pp. 1918–1924, Nov. 1968, doi: 10.1109/TPAS.1968.292013.

[15] S. Jia, R. Qu, and J. Li, 'Analysis of the Power Factor of Stator DC-Excited Vernier Reluctance Machines', *IEEE Transactions on Magnetics*, vol. 51, no. 11, pp. 1–4, Nov. 2015, doi: 10.1109/TMAG.2015.2450493.

[16] I. M. Sobol′, 'Global sensitivity indices for nonlinear mathematical models and their Monte Carlo estimates', *Mathematics and Computers in Simulation*, vol. 55, no. 1, pp. 271–280, Feb. 2001, doi: 10.1016/S0378-4754(00)00270-6.

[17] A. Saltelli, P. Annoni, I. Azzini, F. Campolongo, M. Ratto, and S. Tarantola, 'Variance based sensitivity analysis of model output. Design and estimator for the total sensitivity index', *Computer Physics Communications*, vol. 181, no. 2, pp. 259–270, Feb. 2010, doi: 10.1016/j.cpc.2009.09.018.

[18] D. Wu and Z. Q. Zhu, 'Design Tradeoff Between Cogging Torque and Torque Ripple in Fractional Slot Surface-Mounted Permanent Magnet Machines', *IEEE Transactions on Magnetics*, vol. 51, no. 11, pp. 1–4, Nov. 2015, doi: 10.1109/TMAG.2015.2436714.

[19] X. Zhu, W. Hua, Z. Wu, W. Huang, H. Zhang, and M. Cheng, 'Analytical Approach for Cogging Torque Reduction in Flux-Switching Permanent Magnet Machines Based on Magnetomotive Force-Permeance Model', *IEEE Transactions on Industrial Electronics*, vol. 65, no. 3, pp. 1965–1979, Mar. 2018, doi: 10.1109/TIE.2017.2739688.

[20] Y. Wang, M. J. Jin, W. Z. Fei, and J. X. Shen, 'Cogging torque reduction in permanent magnet flux-switching machines by rotor teeth axial pairing', *IET Electric Power Applications*, vol. 4, no. 7, pp. 500–506, Aug. 2010, doi: 10.1049/iet-epa.2009.0205.

[21] X. Li, F. Shen, S. Yu, and Z. Xue, 'Flux-Regulation principle and performance analysis of a novel axial partitioned stator hybrid-excitation flux-switching machine using parallel magnetic circuit', *IEEE Transactions on Industrial Electronics*, pp. 1–1, 2020, doi: 10.1109/TIE.2020.3001807.

[22] K. Deb, A. Pratap, S. Agarwal, and T. Meyarivan, 'A fast and elitist multiobjective genetic algorithm: NSGA-II', *IEEE Transactions on Evolutionary Computation*, vol. 6, no. 2, pp. 182–197, Apr. 2002, doi: 10.1109/4235.996017.

[23] M.-T. Pham, D. Zhang, and C. S. Koh, 'Multi-Guider and Cross-Searching Approach in Multi-Objective Particle Swarm Optimization for Electromagnetic Problems', *IEEE Trans. Magn.*, vol. 48, no. 2, pp. 539–542, Feb. 2012, doi: 10.1109/TMAG.2011.2173559.

VII. BIOGRAPHIES

Wentao Zhang was born in Suzhou, China, in 1995. He received the B.Eng. degree in electrical engineering and its automation from Southeast University, Nanjing, China, in July 2018. Since September 2018, he has been working toward the M.Sc. degree in the same institute.

His major research interests include the design, analysis, and control of the wound field switched flux machines.

Zhongze Wu (M'18) received the B.Eng. and M.Sc. degrees in electrical engineering from Southeast University, Nanjing, China, in 2010 and 2013, respectively, and the Ph.D. degree in electrical and electronic engineering from The University of Sheffield, Sheffield, U.K., in January 2017.

Since August 2018, he has been with The Institute for Advanced Automotive Propulsion Systems (IAAPS), Department of Mechanical Engineering, University of Bath, Bath, U.K., where he was a Prize Fellow and is currently a Lecturer. His major research interests include the advanced electrical machines and drives for electric propulsion systems.

From January 2017 to August 2018, he was with Warwick Manufacturing Group (WMG), University of Warwick, Coventry, U.K., as a research fellow in electrical machines.

Wei Hua (M'03-SM'16) received the B.Sc. and Ph.D. degrees in electrical engineering from Southeast University, Nanjing, China, in 2001 and 2007, respectively. From 2004 to 2005, he was with the Department of Electronics and Electrical Engineering, The University of Sheffield, U.K., as a Joint-Supervised Ph.D. Student.

Since 2007, he has been with Southeast University, where he is currently a Chief Professor of Southeast University and a Distinguished Professor of Jiangsu Province. He has co-authored over 150 technical papers. He holds 50 patents in his areas of interest. His teaching and research interests include design, analysis, and control of electrical machines, especially for PM brushless machines and switching reluctance machines, etc.

Z. Q. Zhu (M'90–SM'00–F'09) received the B.Eng. and M.Sc. degrees in electrical and electronic engineering from Zhejiang University, Hangzhou, China, in 1982 and 1984, respectively, and the Ph.D. degree in electrical and electronic engineering from The University of Sheffield, Sheffield, U.K., in 1991.

Since 1988, he has been with The University of Sheffield, where he is currently a Research Chair of the Royal Academy of Engineering/Siemens with the Department of Electronic and Electrical Engineering and the Head of the Electrical Machines and Drives Research Group. His current research interests include the design and control of permanent-magnet brushless machines and drives for applications ranging from automotive through domestic appliances to renewable energy.

Dr. Zhu is a Fellow of the Royal Academy of Engineering.